Rarefaction shock in plasma with a bi-Maxwellian electron distribution function

A. Diaw and P. Mora*
Centre de Physique Théorique, École Polytechnique, CNRS, FR-91128 Palaiseau, France
(Received 24 May 2011; published 7 September 2011)

The one-dimensional collisionless expansion into a vacuum of a plasma with a bi-Maxwellian electron distribution function and a single ion species is studied both theoretically and numerically. A shock wave occurs when the ratio of the temperatures between the hot and the cold electrons is larger than $5+\sqrt{24}$ [B. Bezzerides, D. W. Forslund, and E. L. Lindman, Phys. Fluids **21**, 2179 (1978)]. The theoretical model presented here gives a coherent and complete description of the rarefaction shock and its effects on the ion acceleration process. Analytical expressions of the characteristics of the shock are given. The analytical findings are compared to the results of a hybrid code describing the plasma expansion, and an excellent agreement is obtained.

DOI: 10.1103/PhysRevE.84.036402 PACS number(s): 52.35.Tc, 52.30.Ex, 52.38.Kd, 52.65.Ww

I. INTRODUCTION

The physics of the interaction of ultraintense lasers with matter, transformed instantaneously into a very hot plasma, involves various nonlinear phenomena, which occur on very short time scales. A general consequence is the generation of fast electrons (hot electrons) with potentially relativistic velocities coexisting with low energy electrons [1]. In thin foil experiments, the hot electrons can accelerate ions to high energy by causing the foil to expand [2–4].

By studying the expansion of a plasma with electrons described by a bi-Maxwellian distribution function (with hot and cold electron temperatures T_h and T_c, respectively), Wickens *et al*. [5] noticed the possibility of a breakdown of the quasineutrality assumption when the ratio T_h/T_c is greater than $5+\sqrt{24}$, and Bezzerides *et al*. [6] demonstrated theoretically the existence of a rarefaction shock wave in such conditions. Our aim here is to extend these studies in order to give a complete description of the rarefaction shock wave.

This paper is organized as follows. In Sec. II, we present the general equations governing the one-dimensional collisionless plasma expansion into a vacuum and look for a self-similar solution in the quasineutral limit. The conditions required for the occurrence of a rarefaction shock wave are given, and the equations describing the shock and the charge-separation effect inside the shock are written. In Sec. III, the case of a plasma with a bi-Maxwellian electron distribution function with a single ion species is presented in detail. The different regimes for which a rarefaction shock can occur in the plasma are investigated with respect to the ratio of the hot electron density to the cold electron density in the unperturbed plasma. Analytical expressions of the parameters of the rarefaction shock wave are derived by performing expansions for a large ratio of T_h/T_c. Particular attention is paid to the speed of the rarefaction shock compared to the acoustic velocity. Section IV is devoted to the numerical simulations performed with a one-dimensional hybrid code and to their comparison with the results of the analytical model. Finally, the influence of the rarefaction shock wave on the ion acceleration and ion spectrum is discussed.

*patrick.mora@cpht.polytechnique.fr

II. PLASMA EXPANSION

A. General equations

We first recall the general equations describing the plasma expansion, following Bezzerides *et al*. [6]. We consider at $t=0$ a one-dimensional plasma composed of cold ions of mass m_i and charge Ze, occupying the half-space $x\leqslant 0$ with uniform density n_u/Z (in the following the subscript u will always correspond to the unperturbed plasma), and of electrons in equilibrium with the electric potential $\phi(x,t=0)$ that builds up due to the charge separation at the plasma edge, with density $n_e(\phi)$ and pressure $P(\phi)$. We assume that the potential vanishes in the unperturbed plasma ($x<0, |x|\to\infty$), with $n_e(0)=n_u$.

For $t>0$, the ion's motion is described by the fluid equations, which can be written as

$$\frac{\partial n}{\partial t}+\frac{\partial (nv)}{\partial x}=0, \tag{1}$$

$$\frac{\partial v}{\partial t}+v\frac{\partial v}{\partial x}=-\frac{e}{m}\frac{\partial \phi}{\partial x}, \tag{2}$$

where $n(x,t)$ is the ion density multiplied by Z, $v(x,t)$ is the ion velocity, $m=m_i/Z$, and where $\phi(x,t)$ is now time dependent.

Due to the smallness of their mass, the electrons are assumed to stay in equilibrium with the electric potential $\phi(x,t)$, at any position and time, with the same functions $n_e(\phi)$ and $P(\phi)$ as initially. The equilibrium condition reads as

$$n_e(\phi)=\frac{1}{e}\frac{dP}{d\phi}, \tag{3}$$

or, equivalently, considering P as a function of x and t,

$$\frac{\partial \phi}{\partial x}=\frac{1}{en_e}\frac{\partial P}{\partial x}. \tag{4}$$

Finally, the electric potential satisfies Poisson's equation

$$\frac{\partial^2\phi}{\partial x^2}=\frac{e}{\epsilon_0}(n_e-n). \tag{5}$$

B. Self-similar solution

If the local scale length $n/(\partial n/\partial x)$ is much larger than the local Debye length $\lambda_D=[\epsilon_0/e(dn_e/d\phi)]^{1/2}$, we can assume

quasineutrality and write $n = n_e(\phi)$. We can then look for a self-similar solution where the similarity parameter is $\xi = x/t$. The fluid equations of ions simplify to

$$(v-\xi)\frac{dn}{d\xi} = -n\frac{dv}{d\xi}, \tag{6}$$

$$(v-\xi)\frac{dv}{d\xi} = -\frac{c_s^2}{n}\frac{dn}{d\xi}, \tag{7}$$

where

$$c_s^2 = \frac{n_e}{dn_e/d\varphi} = \frac{1}{m}\frac{dP}{dn_e}, \tag{8}$$

for which we have defined $\varphi = e\phi/m$.

When $dn/d\xi \neq 0$, Eqs. (6) and (7) combine to give

$$(v-\xi)^2 = c_s^2. \tag{9}$$

The solution corresponding to an expansion toward $x > 0$ is thus given by

$$v = \xi + c_s, \tag{10}$$

while the electric potential and the position ξ are related by the equation

$$\frac{d\xi}{d\varphi} = -\left(\frac{1}{c_s} + \frac{dc_s}{d\varphi}\right). \tag{11}$$

The right-hand side of Eq. (11) is normally negative and the full solution is obtained by integrating it to obtain ξ as a function of φ. However, if the right-hand side of Eq. (11) happens to be positive for some values of φ, i.e., if

$$c_s\frac{dc_s}{d\varphi} \leqslant -1, \tag{12}$$

one ends up with a mathematical solution where φ is a multivalued function of ξ for a range of values. Physically, a rarefaction shock appears, as discussed by Bezzerides *et al.* [6].

C. Rarefaction shock

Let ξ_s be the self-similar parameter corresponding to the position of the shock. We may treat the shock as a stationary discontinuity in the frame moving with the shock. The equations of conservation of mass and energy flux in this frame read as

$$\frac{d}{dx}(nu) = 0, \tag{13}$$

$$\frac{d}{dx}\left(\frac{1}{2}u^2 + \varphi\right) = 0, \tag{14}$$

where $u = v - \xi_s$ is the relative velocity. To write the momentum conservation equation, one has to take into account the charge separation inside the shock. Multiplying Eq. (14) by n, and using Eqs. (3), (5), and (13), one obtains

$$\frac{d}{dx}\left[nu^2 + \frac{P}{m} - \frac{\epsilon_0 m}{2e^2}\left(\frac{d\varphi}{dx}\right)^2\right] = 0. \tag{15}$$

The jump conditions are

$$n_0u_0 = n_1u_1, \tag{16}$$

$$\tfrac{1}{2}u_0^2 + \varphi_0 = \tfrac{1}{2}u_1^2 + \varphi_1, \tag{17}$$

where the subscripts 0 and 1 denote the conditions upstream and downstream of the shock, respectively, and

$$n_0u_0^2 + \frac{P_0}{m} = n_1u_1^2 + \frac{P_1}{m}, \tag{18}$$

where we have taken into account the fact that the term involving the square of the electric field in Eq. (15) is of order $1/(\omega_{pi0}t)^2$ on the upstream side, for which $\omega_{pi0} = (n_0e^2/m\epsilon_0)^{1/2}$ is the ion plasma frequency, and anticipated the fact that it vanishes on the downstream side, thus neglecting both terms in our analysis, assuming $\omega_{pi0}t \gg 1$.

The conservation equations across the discontinuity combine in the Hugoniot relation

$$\varphi_0 - \varphi_1 = \left(\frac{P_0 - P_1}{2m}\right)\left(\frac{1}{n_0} + \frac{1}{n_1}\right). \tag{19}$$

Inside the shock, the electrostatic energy can be deduced from Eqs. (13), (14), and (15), resulting in

$$\frac{\epsilon_0 m}{2e^2}\left(\frac{d\varphi}{dx}\right)^2 = F(\varphi), \tag{20}$$

with

$$F(\varphi) = n_0u_0\sqrt{u_0^2 + 2(\varphi_0 - \varphi)} - n_0u_0^2 + \frac{P - P_0}{m}. \tag{21}$$

The function $F(\varphi)$ verifies

$$\frac{dF(\varphi)}{d\varphi} = n_e - n \tag{22}$$

and

$$\frac{d^2F(\varphi)}{d\varphi^2} = \frac{n_e}{c_s^2} - \frac{n}{u^2}. \tag{23}$$

The function $F(\varphi)$ and its first derivative vanish on both sides of the discontinuity (as the electric field and the charge separation do), but $F(\varphi)$ has to be positive in the interval $\varphi_1 < \varphi < \varphi_0$, which implies that the second derivative of $F(\varphi)$ has to be $\geqslant 0$ both for φ_0 and φ_1, meaning that the flow has to be sonic or supersonic on both sides of the discontinuity, i.e.,

$$u_0 \geqslant c_{s0}, \quad u_1 \geqslant c_{s1}. \tag{24}$$

On the other hand, at the position of the maximum of the electric field, $dF(\varphi)/d\varphi$ vanishes and the second derivative $d^2F(\varphi)/d\varphi^2$ has to be negative, which means that the flow has to be subsonic at this point.

An alternate way to define an acoustic velocity is by reference to the ion density instead of the electron density, with

$$c_{si}^2 = \frac{1}{m}\frac{dP}{dn}. \tag{25}$$

The two velocities c_s and c_{si} coincide in the quasineutral part of the expansion, but differ inside the shock. Differentiating

Eq. (21) and using Eq. (22) and the conservation of mass flux, one obtains inside the shock

$$c_{si} = \sqrt{\frac{n_e}{n}}\, u. \tag{26}$$

With this definition of the acoustic velocity, the flow is sonic both on the upstream and on the downstream sides. Inside the shock, it first becomes subsonic and then supersonic, as we will illustrate in the case of a bi-Maxwellian electron distribution function.

III. CASE OF A BI-MAXWELLIAN ELECTRON DISTRIBUTION FUNCTION

We now consider the case of a bi-Maxwellian electron population, with

$$\begin{aligned} n_e(\phi) &= n_h(\phi) + n_c(\phi) \\ &= n_{hu} \exp\left(\frac{e\phi}{k_B T_h}\right) + n_{cu} \exp\left(\frac{e\phi}{k_B T_c}\right), \end{aligned} \tag{27}$$

where k_B is the Boltzmann constant, T_h and T_c are, respectively, the hot and cold temperatures, and n_{hu} and n_{cu} are the corresponding densities in the unperturbed plasma, with $n_{hu} + n_{cu} = n_u$.

The ion acoustic velocity is

$$c_s(y) = c_{sh}\sqrt{\frac{1+y}{\alpha+y}}, \tag{28}$$

where $c_{sh} = \sqrt{k_B T_h/m}$ is the sound velocity associated with hot electrons only, and

$$\alpha = T_h/T_c, \quad y(\phi) = n_h/n_c. \tag{29}$$

As shown by both Wickens *et al.* [5] and by Bezzerides *et al.* [6], a necessary condition for Eq. (12) to be valid is $\alpha \geqslant 5 + \sqrt{24} \approx 9.9$. Figure 1 shows the electric potential normalized to $k_B T_h/e$ as a function of ξ/c_{sh} precisely for the critical temperature ratio $\alpha = 5 + \sqrt{24}$ and a density ratio $y_u = y(0) = n_{hu}/n_{cu} = 0.1$. In this case, the derivative $d\xi/d\varphi$ vanishes at a position where $y = 5 + \sqrt{24}$. Note that this occurs only when y_u is smaller than this critical value.

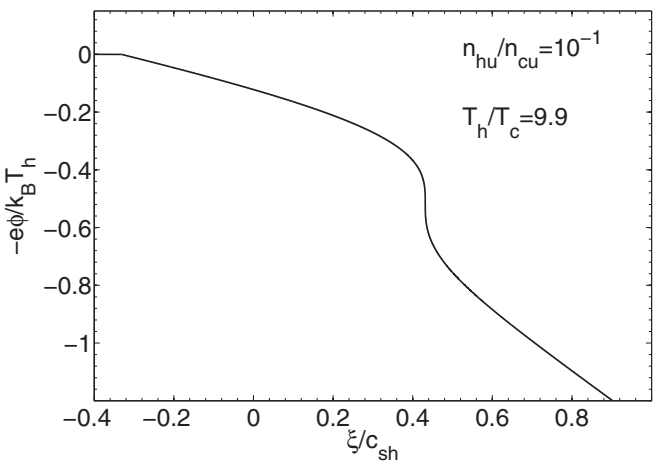

FIG. 1. Electric potential ϕ as a function of ξ, calculated by numerical integration of Eq. (11). The parameters are $\alpha = T_h/T_c = 5 + \sqrt{24} \approx 9.9$ and $y_u = n_{hu}/n_{cu} = 0.1$.

A. Rarefaction shock: Standard case

Figure 2 shows the solution of Eq. (11) for $\alpha = 10^2$ and $y_u = 10^{-2}$. The portion of the curve between C and D corresponds to the values of φ for which the condition (12) is true. Also shown in Fig. 2 is the physical solution obtained by using the jump conditions (16)–(18) with the constraint (24). The following regions are identified: the unperturbed plasma on the left of the rarefaction wave situated in A, an expansion dominated by cold electrons between A and B, the shock rarefaction joining B and E, a plateau between E and F, and an expansion dominated by hot electrons on the right of F. Contrary to what was supposed by Wickens and Allen [7], the discontinuity does not coincide with the first occurrence of the singular point on the multivalued self-similar solution. In other words, the discontinuity occurs before reaching C.

The Hugoniot relation (19) can be written as

$$\begin{aligned} w = \frac{1}{2}&\left[y_0(1-e^{-w}) + \frac{1}{\alpha}(1-e^{-\alpha w})\right] \\ &\times \left(\frac{1}{y_0+1} + \frac{1}{y_0 e^{-w} + e^{-\alpha w}}\right), \end{aligned} \tag{30}$$

where $w = e(\phi_0 - \phi_1)/k_B T_h$, $y_0 = n_{h0}/n_{c0}$, $n_{h0} = n_h(\phi_0)$, and $n_{c0} = n_c(\phi_0)$. Given w (>0 for a rarefaction), Eq. (30) is a quadratic equation for y_0, which has two positive solutions provided that w is not too large. The upstream and downstream velocities are

$$u_0 = c_{sh}\left[\frac{2w}{\left(\frac{y_0+1}{y_0 e^{-w}+e^{-\alpha w}}\right)^2 - 1}\right]^{1/2} \tag{31}$$

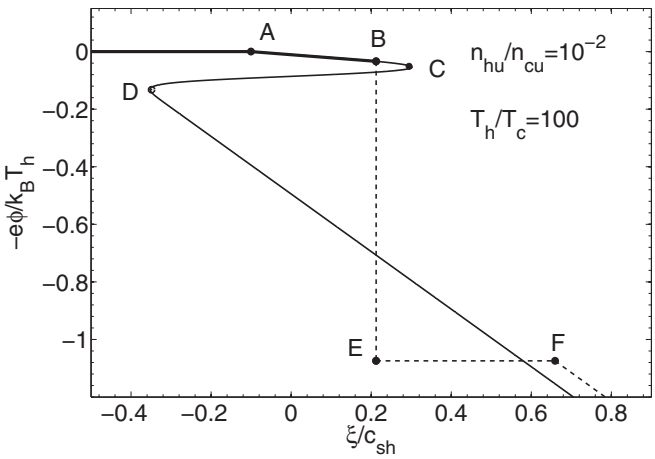

FIG. 2. Electric potential ϕ (solid line) as a function of ξ, calculated by numerical integration of Eq. (11), for $\alpha = 10^2$ and $y_u = 10^{-2}$. Also shown (dashed line) is the physical solution obtained by using the jump conditions (16)–(18) with the constraint (24). The upper part, down to point B (thick black line), is common to the two solutions.

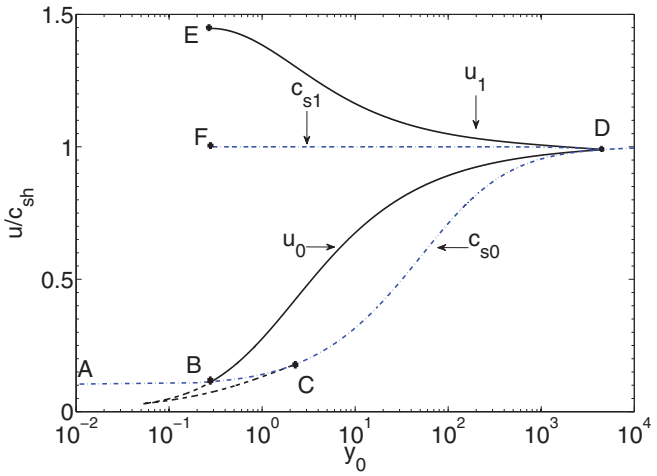

FIG. 3. (Color online) Ion velocity as a function of the electrons density ratio y_0 upstream of the shock for a temperature ratio $\alpha = 10^2$. The dotted-dashed blue lines represent the sound velocity upstream c_{s0} and downstream c_{s1} of the shock. The solid black lines are the ion velocity upstream u_0 and downstream u_1 of the shock. The dashed line represents the values of u_0 for which the constraint (24) is not fulfilled.

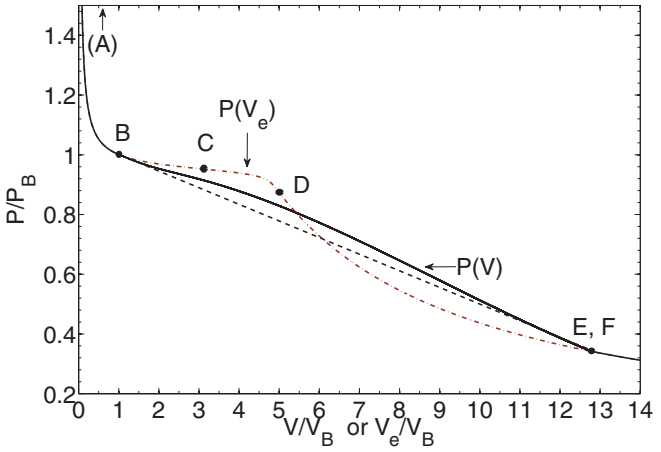

FIG. 4. (Color online) Electron pressure as a function of the electron specific volume $V_e = 1/n_e$ (dotted-dashed brown line) and of the ion specific volume $V = 1/n$ (solid line) for $\alpha = 10^2$. The points A–F identified in the plasma expansion in Fig. 2 are also shown. The dashed line is the straight line connecting B to E. The specific volumes V_e and V and the pressure P are normalized to their values on the upstream side of the shock (point B).

and

$$u_1 = \sqrt{u_0^2 + 2w\, c_{sh}^2}. \tag{32}$$

The upstream velocity u_0 is plotted in Fig. 3 as a function of y_0 for $\alpha = 10^2$. Also shown is the upstream sound velocity c_{s0}. The solutions for which $u_0 < c_{s0}$ (which would correspond to a plateau on the upstream side) are plotted as dashed lines, as they violate the constraint (24) and, thus, do not correspond to a physical solution. Also shown are the downstream velocity u_1 and the downstream sound velocity c_{s1} (only drawn for the physical solution).

Let us now discuss the position of the upstream point B of Fig. 2 on the graph of Fig. 3. First of all, B must correspond to a solution of the Hugoniot equation. Second, it also belongs to the rarefaction expansion dominated by the cold electrons, with $v_0 = \xi_s + c_{s0}$ and thus $u_0 = c_{s0}$. As a result, point B is at the intersection of the Hugoniot curve $u_0(y_0)$ and of the sonic curve $c_{s0}(y_0)$, so that, combining Eqs. (28) and (31), one has

$$w = \frac{1}{2}\frac{1+y_0}{\alpha+y_0}\left[\left(\frac{1+y_0}{y_0 e^{-w} + e^{-\alpha w}}\right)^2 - 1\right]. \tag{33}$$

B. Detailed structure of the shock

Figure 4 shows the P, V_e and the P, V diagrams (where $V_e = 1/n_e$ and $V = 1/n$) of the rarefaction shock for a temperature ratio $\alpha = 10^2$. The points A–F identified in the plasma expansion in Fig. 2 are also shown. The two curves coincide on the left of B and on the right of points E, F, where the flow is quasineutral. The dashed line is the straight line connecting B to E, and corresponds to the equation

$$nu^2 + \frac{P}{m} = n_0 u_0^2 + \frac{P_0}{m}, \tag{34}$$

with $nu = n_0 u_0$. The difference between the curve $P(V)$ (black line) and the straight dashed line is simply proportional to the electrostatic energy density in the shock. The three curves are tangents at point B, which is related to the fact that the sound velocities c_s and c_{si} coincide and are equal to the upstream flow velocity u_0. At point E (but on the left of point E), the tangent to the curve $P(V)$ coincides with the dashed line, which is due to the fact that the sound velocity c_{si} coincides with the downstream flow velocity u_1, but differs from the tangent of the curve $P(V_e)$. This can be explained by the fact that the two sound velocities differ on the left of point E, and that the flow is supersonic in the sense that $u_1 > c_s$.

If we now consider the function $P(V)$ on both sides of point E, we observe that its derivative is discontinuous, which means that the sound velocity c_{si} is discontinuous. Thus, two characteristics C_- with different slopes emanate from the break point E, leading to the formation of a plateau, the length of which is given by $\Delta c_{si} t$, where $\Delta c_{si} = c_{si} - c_s$ is the difference between the two sound velocities. Note the similarities with the case of a rarefaction shock wave in a medium undergoing a phase transition with $(\partial^2 P/\partial V^2)_s < 0$, as discussed schematically by Bethe [8] and in more details by Zel'dovich and Raizer [9]. Here, the condition (12) instead reads as $(\partial^2 P/\partial V_e^2)_{T_h, T_c} < 0$, and the break point is on the downstream side, not on the upstream side.

Once the shock parameters are known, it is possible to determine the structure of the electric field $E = -\partial\phi/\partial x$ in the rarefaction shock by solving Eq. (20) with the appropriate boundary conditions. The result is given in Figs. 5(a) and 5(b), where ϕ and E are shown as functions of $X \approx x - \xi_s t$ for a temperature ratio $\alpha = 10^2$. The position is normalized to the local Debye length $\lambda_{Dh0} = \sqrt{\epsilon_0 k_B T_h / n_{h0} e^2}$, and the position

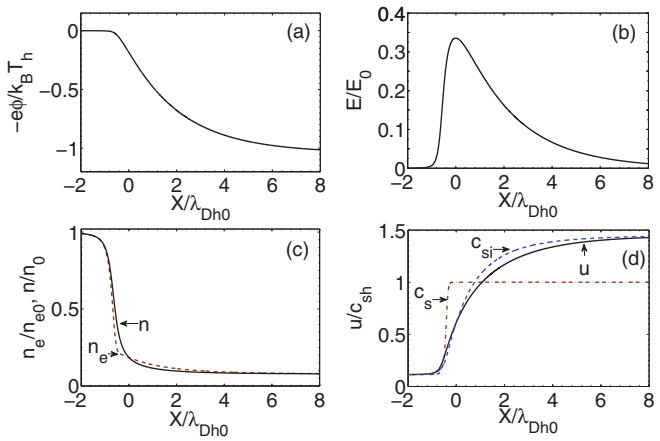

FIG. 5. (Color online) (a), (b) Profiles of the potential and the electric field in the shock wave. (c) Profiles of the ion and electron densities. (d) Profiles of the ion sound velocities and of the velocity of the ion stream. All profiles correspond to the standard case of Fig. 2, with $\alpha = 10^2$. The electric field is normalized to $E_0 = \sqrt{n_{h0} k_B T_h/\epsilon_0}$. The position $X \approx x - \xi_s t$ is normalized to the Debye length $\lambda_{Dh0} = \sqrt{\epsilon_0 k_B T_h/n_{h0} e^2}$, with $X = 0$ corresponding to the maximum of the electric field.

$X = 0$ has been arbitrarily assigned to the position of the maximum of the electric field.

Figure 5(c) shows the corresponding ion and electron densities' profiles in the rarefaction shock as functions of X. Finally, Fig. 5(d) shows the profiles of the ion velocity and of the acoustic velocity. One observes that the flow, which is sonic upstream, becomes successively supersonic, subsonic, and supersonic (here we refer to the ratio of the flow velocity u to the acoustic velocity c_s).

C. Asymptotic expressions for $\alpha \gg 1$

For a large temperature ratio $\alpha \gg 1$, it is possible to obtain asymptotic expressions for the quantities characterizing the plasma expansion. Here, we complete or correct expressions given in [6,10,11]. First of all, the rarefaction wave enters the unperturbed plasma at the sound velocity $c_s(y_u)$, so that

$$\xi_A \approx -\left(1 + \frac{y_u}{2}\right) \frac{c_{sh}}{\sqrt{\alpha}}. \tag{35}$$

In Fig. 2, the points C and D between which the solution of Eq. (11) has a nonphysical slope are such that

$$y_C \approx 2\left(1 + \frac{6}{\alpha}\right) \tag{36}$$

and

$$y_D \approx \frac{\alpha^2}{2}\left(1 - \frac{6}{\alpha}\right). \tag{37}$$

The sound velocity in the upstream region is given by

$$c_s \approx \left(1 + \frac{y}{2}\right) \frac{c_{sh}}{\sqrt{\alpha}}. \tag{38}$$

The position of the rarefaction shock ξ_s is obtained by using Eq. (38) to integrate Eq. (11) between ξ_A and ξ_s, which gives

$$\xi_s \approx \left[\ln\left(\frac{y_0}{y_u}\right) + \frac{y_u}{2} - y_0 - 1\right] \frac{c_{sh}}{\sqrt{\alpha}}. \tag{39}$$

The upstream density ratio y_0 and the potential jump w are obtained by looking for expansions of both quantities as powers of the small parameter $1/\sqrt{\alpha}$, inserting these expansions into Eqs. (30) and (33), and solving order by order. The results are (keeping only the leading two terms)

$$w \approx 1.26 - \frac{2.10}{\sqrt{\alpha}}, \tag{40}$$

$$y_0 = y_B \approx \frac{2.22}{\sqrt{\alpha}} + \frac{4.57}{\alpha}, \tag{41}$$

while the downstream density ratio $y_1 = y_E = y_F = y_0 \exp(1-\alpha)w$ is completely negligible. The upstream velocity u_0 coincides with the sound velocity in B,

$$u_0 \approx \left(1 + \frac{1.11}{\sqrt{\alpha}}\right) \frac{c_{sh}}{\sqrt{\alpha}}. \tag{42}$$

The downstream velocity is

$$u_1 \approx \left(1.59 - \frac{1.32}{\sqrt{\alpha}}\right) c_{sh}. \tag{43}$$

Finally, the position of point F, where the expansion dominated by the hot electrons begins, is given by

$$\xi_F \approx \xi_s + \left(0.59 - \frac{1.32}{\sqrt{\alpha}}\right) c_{sh}. \tag{44}$$

D. Supersonic rarefaction shock case

When $y_u = y_B$, the analysis of Secs. III A–III C still applies, although the region of expansion dominated by the cold electrons (line A-B in Fig. 2) disappears, and A and B become

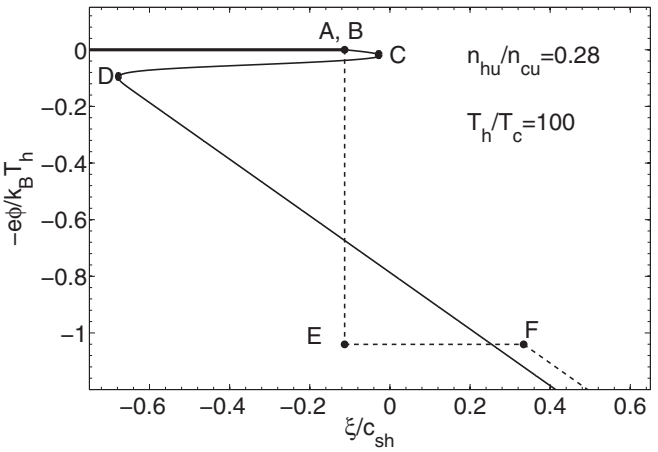

FIG. 6. Electric potential ϕ (solid line) as a function of ξ, calculated by numerical integration of Eq. (11), for $\alpha = 10^2$ and for the transition value $y_u = y_B \approx 0.28$. Also shown (dashed line) is the physical solution obtained by using the jump conditions (16)–(18) with the constraint (24).

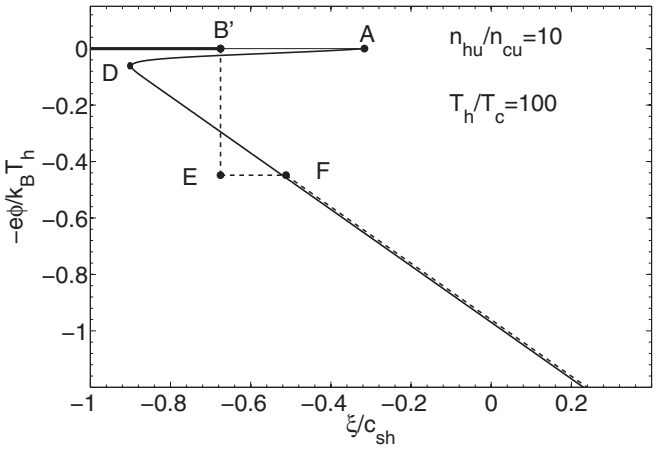

FIG. 7. Electric potential ϕ (solid line) as a function of ξ, calculated by numerical integration of Eq. (11), for $\alpha = 10^2$ and $y_u = 10$. Also shown (dashed line) is the physical solution obtained by using the jump conditions (**??**) with the constraint (24).

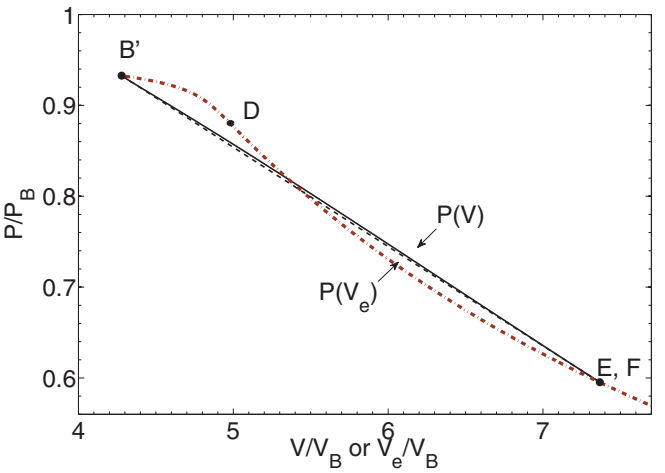

FIG. 9. (Color online) Same as Fig. 4, with the points B', D, E, and F corresponding to the parameters of of Fig. 7, i.e, $\alpha = 10^2$ and $y_u = 10$.

merged. The unperturbed plasma is directly connected to the rarefaction shock, which propagates inside the unperturbed plasma at the sonic velocity. This is illustrated in Fig. 6.

For $y_u > y_B$ (and still $y_u < y_D$), the structure of the expansion becomes different, as illustrated in Fig. 7, which plots the electric potential ϕ as a function of ξ for $\alpha = 100$ and $y_u = 10$. The unperturbed plasma is again directly connected to the rarefaction shock, but the shock now propagates inside the plasma at a supersonic velocity, as its position B' is further inside the plasma than the position A of a virtual sound wave.

Furthermore, one can note that, in contrast with the cases where $y_u < y_B$, the potential jump and the width of the plateau now become smaller and smaller as y_u increases.

The Hugoniot relation (30) is still valid, with y_0 now given by y_u. Figure 8 is identical to Fig. 3, except that the positions of the points A, B', E, and F corresponding to the parameters of Fig. 7, i.e., $\alpha = 10^2$ and $y_u = 10$, have been added. In the same way, Fig. 9 is similar to Fig. 4 with the positions of the points B',D, E, and F corresponding to the parameters of Fig. 7.

In B', the slope of the curve $P(V)$ is larger than the slope of the curve $P(V_e)$. This can be understood by the fact that $u_0(=c_{si}) > c_s$ and that the rarefaction shock propagates at a supersonic velocity inside the unperturbed plasma.

On the downstream side, the situation is similar to that of the standard case, except that the difference of the values of the slopes of the two curves $P(V)$ and $P(V_e)$ in E,F is smaller, implying a smaller plateau length.

In the limit $\alpha \gg 1$, Eqs. (28), (30), and (31) can be simplified by neglecting terms of order $1/\alpha$ or $e^{-\alpha w}$, giving

$$c_s(y_u) \approx c_{sh}\sqrt{\frac{1+y_u}{\alpha}}, \tag{45}$$

$$w = \frac{1}{2}(1-e^{-w})\left(\frac{y_u}{y_u+1} + e^{w}\right), \tag{46}$$

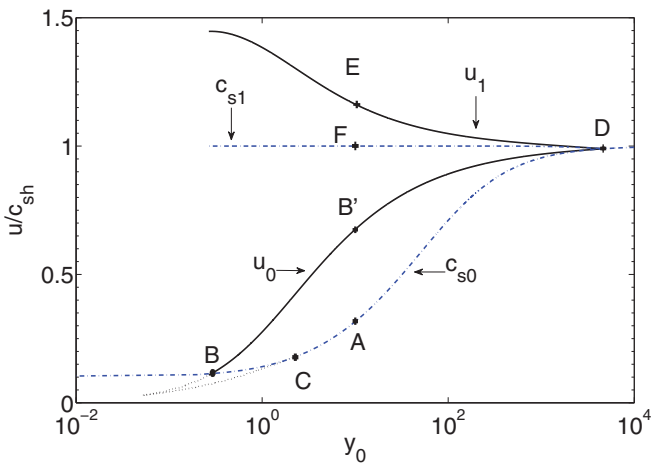

FIG. 8. (Color online) Same as Fig. 3, with the positions of the points A, B', E, and F corresponding to the parameters of Fig. 7, i.e., $\alpha = 10^2$ and $y_u = 10$.

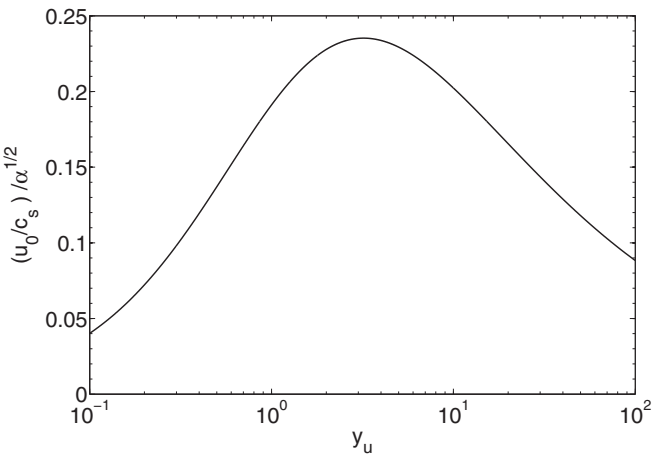

FIG. 10. Ratio of the upstream velocity to the acoustic velocity in the unperturbed plasma, as a function of the density ratio y_u, in the supersonic rarefaction shock case, in the limit $\alpha \gg 1$.

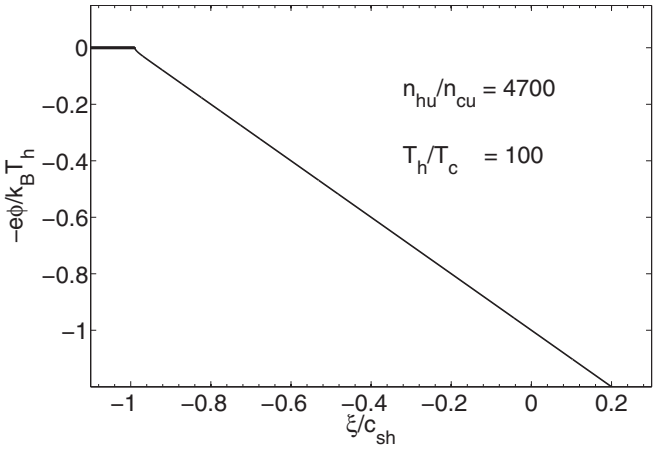

FIG. 11. Electric potential ϕ as a function of ξ, calculated by numerical integration of Eq. (11), for $\alpha = 10^2$ and $y_u = y_D \approx 4700$.

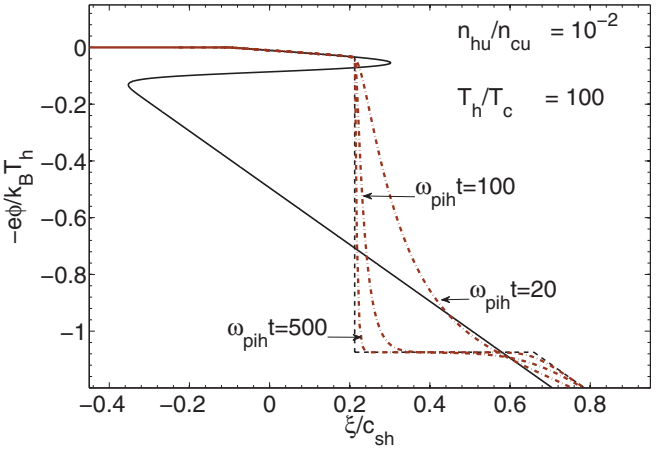

FIG. 12. (Color online) Electric potential ϕ (dotted-dashed brown line) as a function of ξ for $\alpha = 10^2$ and $y_u = 10^{-2}$ and at different times $\omega_{pih}t = 20$, 100, and 500, as obtained with the hybrid code. Also shown (solid line) is the result obtained from the numerical integration of Eq. (11). The dashed line is the result of the analytical model presented in Sec. III.

and

$$u_0 = c_{sh}\left[\frac{2w}{\left(\frac{y_u+1}{y_u}e^w\right)^2 - 1}\right]^{1/2}. \tag{47}$$

The corresponding ratio u_0/c_s is plotted in Fig. 10 as a function of y_u. The ratio is maximal for $y_u \approx 3.2$, for which it reaches $u_0/c_s \approx 0.24\sqrt{\alpha}$ (i.e., $u_0 \approx 0.48 c_{sh}$).

E. Hot electrons rarefaction : $y_u \geqslant y_D$

In the limit $y_u \geqslant y_D$, the cold electrons are almost negligible. Figure 11 shows the electric potential for $\alpha = 10^2$ and $y_u = y_D \approx 4700$. The shock rarefaction completely disappears as expected, and the region of expansion dominated by the hot electrons is directly connected to the unperturbed plasma. The parameters of the expansion can be expressed with the self-similar model with a single hot electron population, with

$$e\phi/k_B T_h \approx -(1 + x/c_{sh}t). \tag{48}$$

IV. NUMERICAL SIMULATIONS

A. General features of the code

Numerical simulations were made with the collisionless one-dimensional hybrid code described in [12]. In this code, the ions are treated as macroparticles, the electrons are treated as a fluid with a density determined by a given function $n_e(\phi)$, and the nonlinear Poisson equation is solved iteratively. Such a code has been used in similar conditions in Ref. [13]. Here, the electrons satisfy Eq. (27) with T_h and T_c independent of time. The time step Δt is chosen to satisfy the plasma stability and, in most cases, is such that $\omega_{pih}\Delta t = 0.1$, where $\omega_{pih} = (n_{hu}e^2/m\epsilon_0)^{1/2}$ is the ion plasma frequency associated with the hot electrons density in the unperturbed plasma.

B. Simulation results

Figure 12 shows the profile of the electric potential for $\alpha = 10^2$ and $y_u = 10^{-2}$, which are the parameters also used in Figs. 2–5, and for $\omega_{pih}t = 20$, 100, and 500. To facilitate the comparison with Fig. 2, we also show in green the result obtained from the numerical integration of Eq. (11) and in blue the result of the analytical model presented in Sec. III. There is an excellent agreement between the analytical model and the numerical results, in particular for large values of $\omega_{pih}t$.

As discussed in Sec. III B, the width of the shock is determined by the local Debye length. The electric field is shown in Fig. 13 as a function of ξ, for the earlier time $\omega_{pih}t = 20$. Here, the electric field is normalized to $E_u = \sqrt{n_{hu}k_B T_h/\epsilon_0}$. Also shown in the inset is a zoom around the shock position, with E shown as a function of $X' = x - \xi_s t$. For ease of comparison, the same normalizations are used in the inset as in Fig. 5(b). With the parameters of the simulation, $n_{h0} \approx 0.967 n_{hu}$, so that the difference between E_u and E_0 is less than 2%.

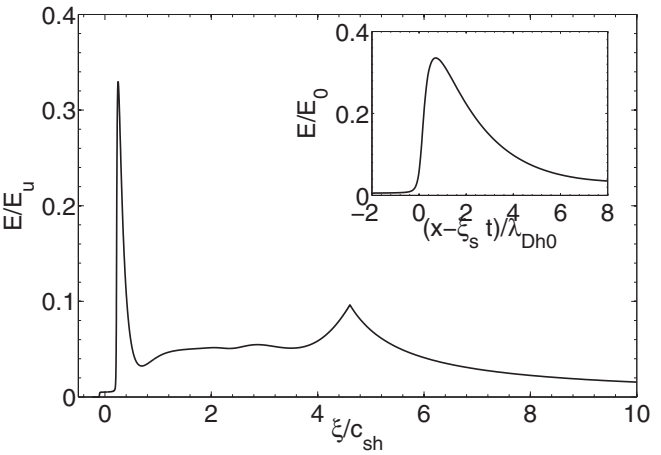

FIG. 13. Electric field as a function of ξ. The parameters of the simulations are $\alpha = 10^2$ and $y_u = 10^{-2}$, and $\omega_{pih}t = 20$. The inset is a zoom around the shock position for an easier comparison with Fig. 5(b). The normalizations are discussed in the text.

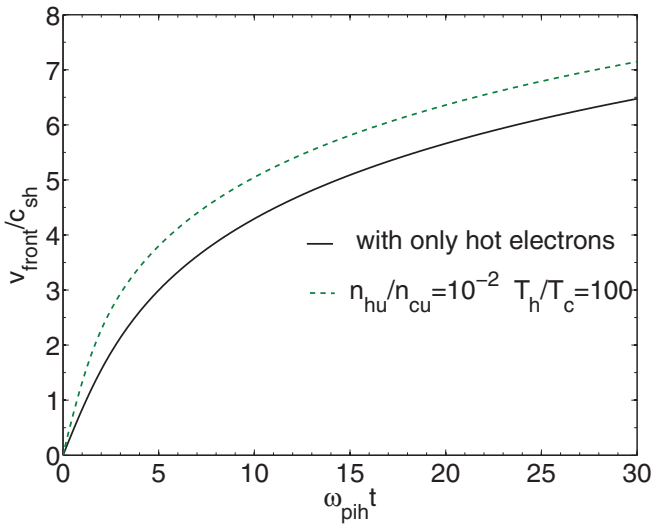

FIG. 14. (Color online) Ion front velocity as a function of time for $\alpha = 10^2$ and $y_u = 10^{-2}$. Also shown is the case where the cold electrons have been suppressed ($y_u = \infty$).

One observes two peaks in the profile of the electric field [14,15]. The first peak, which stands at $x \approx \xi_s t$ (more precisely $X' \approx 0.5\lambda_{Dh0}$), corresponds to the rarefaction shock, and compares favorably with what has been discussed in Sec. III B [compare the inset of Fig. 13 to Fig. 5(b)]. The second peak corresponds to the ion front as discussed in Ref. [16] and observed in Ref. [17]. The first peak is almost independent of time in a ξ, E diagram, while the second peak shifts logarithmically toward large values of ξ with an amplitude going to 0 as $2E_u/\omega_{pih}t$.

The time evolution of the ion front velocity (corresponding to the second peak in Fig. 13) is illustrated in Fig. 14 for $\alpha = 10^2$ and $y_u = 10^{-2}$. Also shown is the case where the cold electrons have been suppressed ($y_u = \infty$). One observes that the difference between the two curves is mainly due to the initial phase of the ion acceleration, where the cold

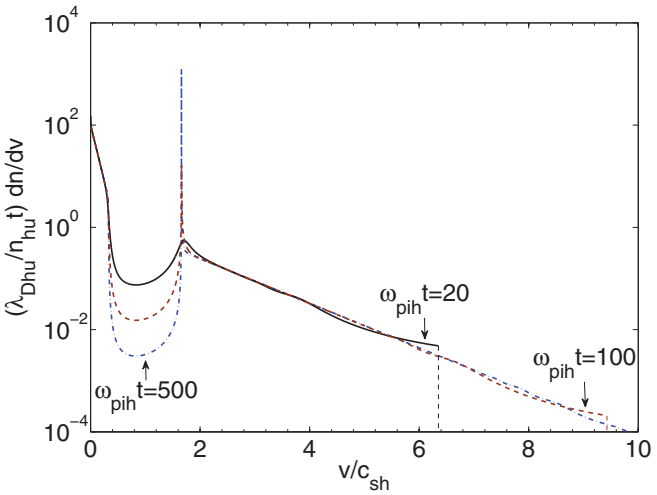

FIG. 15. (Color online) Normalized ion velocity spectrum as a function of time for the same parameters as in Fig. 12, i.e., $\alpha = 10^2$ and $y_u = 10^{-2}$ and for $\omega_{pih}t = 20$, 100, and 500.

electrons slightly enhance the strength of the accelerating field, as discussed for initial time $t = 0$ in Refs. [18,19].

Finally, the velocity spectrum is shown in Fig. 15 for the same parameters as in Fig. 12. The spectrum is normalized to time, as the number of accelerated ions increases almost linearly with time. One recognizes on the spectrum the low velocity part corresponding to the expansion dominated by the cold electrons (line A-B in Fig. 2), the dip corresponding to the shock (line B-E), the peak corresponding to the plateau (line E-F), and the high velocity part corresponding to the expansion dominated by hot electrons (right of F) down to the velocity cutoff.

V. CONCLUSION

A complete theory of rarefaction shocks occurring in a plasma with a bi-Maxwellian electron distribution function has been presented in this paper. The existence of the shock results from the breakdown of the self-similar model that happens when the ratio between the hot and the cold electron temperature is larger than $5 + \sqrt{24} \approx 9.9$.

Two main cases were distinguished. In the standard case (Secs. III A–III C), corresponding to low values of the hot electron density in the unperturbed plasma, the plasma can be divided into five different regions: the unperturbed region of the plasma, a zone of expansion dominated by the cold electrons, the rarefaction shock itself, a plateau, and finally a zone of expansion dominated by the hot electrons ending at the ion front. The various quantities characterizing the expansion have been accurately determined. The rarefaction shock structure and the ion front structure are determined by charge-separation effects and involve the local Debye length. The other characteristics of the expansion can be determined by a self-similar analysis and a classical Hugoniot treatment of the discontinuity.

The supersonic rarefaction shock case (Sec. III D) corresponds to intermediate values of the hot electron density in the unperturbed plasma. In this case, the rarefaction shock is directly connected to the unperturbed plasma, and the rarefaction shock propagates inside the plasma at a supersonic velocity.

Numerical simulations with a one-dimensional hybrid code confirmed our findings, and show that the rarefaction shock leads to a dip in the velocity spectrum, the depth of which increases with time. On the other hand, the maximum ion velocity is mainly dependent on the hot electrons component of the electron distribution function.

In our analysis, the unperturbed densities n_{hu} and n_{cu} are assumed to be independent of time, as well as the hot and cold electron temperatures T_h and T_c. This means that the unperturbed plasma is an infinite source of particles and energy. For a finite plasma foil, the number of particles is conserved, and the electron distribution function may vary in time, in particular, due to the energy exchange with ions [13,20]. For instance, it has been shown recently in the case of an initial single Maxwellian distribution function that the electron distribution function is strongly modified by the expansion, resulting in a surprising acceleration of the rarefaction wave in spite of the overall loss of energy of the electrons [21,22]. The corresponding study in the case of an initial bi-Maxwellian distribution function is left for another paper.

[1] S. D. Baton *et al*., Plasma Phys. Controlled Fusion **47**, B777 (2005).
[2] M. Borghesi, J. Fuchs, S. V. Bulanov, A. J. Mackinnon, P. K. Patel, and M. Roth, Fusion Sci. Technol. **49**, 412 (2006).
[3] J. Fuchs *et al*., Nat. Phys. **2**, 48 (2006).
[4] L. Robson *et al*., Nat. Phys. **3**, 58 (2007).
[5] L. M. Wickens, J. E. Allen and P. T. Rumsby, Phys. Rev. Lett. **41**, 243 (1978).
[6] B. Bezzerides, D. W. Forslund and E. L. Lindman, Phys. Fluids **21**, 2179 (1978).
[7] L. M. Wickens and J. E. Allen, J. Plasma Phys. **22**, 167 (1979).
[8] H. A. Bethe, in *Classic Papers in Shock Compression Science*, edited by J. W. Johnson and R. Cheret (Springer, Heidelberg, 1998), p. 417.
[9] Ya. B. Zeldovich and Yu. P. Raizer, *Physics of Shock Waves and High-Temperature Hydrodynamic Phenomena* (Dover, New York, 2002), p. 67 and p. 757.
[10] R. L. Morse and C. W. Nielson, Phys. Fluids **16**, 909 (1973).
[11] V. T. Tikhonchuk, A. A. Andreev, S. G. Bochkarev, and V. Y. Bychenkov, Plasma Phys. Controlled Fusion **47**, B869 (2005).
[12] P. Mora, Phys. Plasmas **12**, 112102 (2005).
[13] P. Mora, Phys. Rev. E **72**, 056401 (2005).
[14] J. Denavit, Phys. Fluids **22**, 1384 (1979).
[15] M. A. True, J. R. Albritton, and E. A. Williams, Phys. Fluids **24**, 1885 (1981).
[16] P. Mora, Phys. Rev. Lett. **90**, 185002 (2003).
[17] L. Romagnani *et al*., Phys. Rev. Lett. **95**, 195001 (2005).
[18] V. Y. Bychenkov, V. N. Novikov, D. Batani, V. T. Tikhonchuk, and S. G. Bochkarev, Phys. Plasmas **11**, 3242 (2004).
[19] M. Passoni, V. T. Tikhonchuk, M. Lontano, and V. Y. Bychenkov, Phys. Rev. E **69**, 026411 (2004).
[20] V. F. Kovalev, V. Yu. Bychenkov, and V. T. Tikhonchuk, Zh. Eksp. Teor. Fiz. **122**, 264 (2002) [Sov. Phys. JETP **95**, 226 (2002)].
[21] T. Grismayer, P. Mora, J. C. Adam, and A. Héron, Phys. Rev. E **77**, 066407 (2008).
[22] P. Mora and T. Grismayer, Phys. Rev. Lett. **102**, 145001 (2009).